Research Article | Vol. 28, No. 26 / 21 December 2020 / Optics Express 38603
Optics EXPRESS

Linearized phase modulated microwave photonic link based on integrated ring resonators

GAOJIAN LIU,[1,2] OKKY DAULAY,[1] QINGGUI TAN,[2] HONGXI YU,[2] AND DAVID MARPAUNG[1,*]

[1]Nonlinear Nanophotonics Group, Laser Physics and Nonlinear Optics (LPNO), Faculty of Science and Technology—University of Twente, PO Box 217, 7500 AE, Enschede, Netherlands
[2]China Academy of Space Technology (Xi'an), Xi'an 710100, China
[*]david.marpaung@utwente.nl

Abstract: An on-chip linearization method for phase modulated microwave photonic link based on integrated ring resonators is proposed. By properly tailoring the phase and amplitude of optical carrier band and second-order sidebands, the third-order intermodulation distortion (IMD3) components can be suppressed. Theoretical analysis are taken and a proof-of-concept experiment is carried out. Experimental results demonstrate that IMD3 is suppressed by 21.7 dB. When the noise of the link is properly optimized, an SFDR of 112.7 dB·Hz$^{2/3}$ can be achieved. This opens the possibility of integrating linearization into a functional photonic integrated circuit.

1. Introduction

Microwave photonic links (MPL) with the advantage of large bandwidth, low loss and immunity to electromagnetic interference have been widely used in antenna remoting, radio-over-fiber and high speed wireless communication [1,2]. Nevertheless MPLs are susceptible to nonlinear distortions, which are induced by the inherent nonlinear transfer function of optoelectronic devices (mainly, modulators). These nonlinear distortions are classified as harmonic distortions and intermodulation distortions. Harmonic distortions can be easily filtered out because they are away from the desired fundamental components. However, the intermodulation distortions, especially the third-order intermodulation distortion (IMD3), are so close to the fundamental components and cannot be filtered easily. IMD3 is the main nonlinearity that will degrade the performance of MPL. Spurious free dynamic range (SFDR) is a figure of merit to evaluate the linearity of MPL. It is a ratio of input power where the lower limit is the input power when the output fundamental signal power is equal to the noise power, the upper limit is the input power when the nth-order intermodulation distortion (IMDn) power is equal to the noise power [3]. By reducing the IMD3, SFDR can be effectively enhanced, which means the linearity of MPL is improved.

Several optical schemes have been proposed to achieve wide bandwidth and highly linear MPL. These methods can mainly be classified into two categories: The first category is using two paths to generate complementary IMD3 terms which will be subtracted at photodetector [4–9]. These complementary paths can be achieved by using dual-wavelength [4–6], dual-polarization state [7,8], or parallel Mach–Zehnder modulator [9]. The second category is direct processing the modulated optical spectrum to reduce the IMD3 components. By processing the phase and amplitude of optical carrier and the sidebands, the IMD3 terms induced by beating between different optical spectrum contributors can cancel each other out [10–14].

Optical spectrum processing method for MPL linearization was first proposed in intensity-modulation (IM) links [10,11]. The phase shift of optical carrier and the nonlinear distortion terms at each side of carrier, namely optical carrier band (OCB), was tailored to suppress

#413392 https://doi.org/10.1364/OE.413392
Journal © 2020 Received 26 Oct 2020; revised 23 Nov 2020; accepted 27 Nov 2020; published 7 Dec 2020

Optics EXPRESS

IMD3 terms, leading to an improved SFDR. Later on, the optical spectrum processing method was implemented in phase modulated (PM) links [12–14], as a PM link has the advantages of eliminating the bias drifting problem and low insertion loss, which can improve the simplicity and reliability of the MWP system.

Implementing optical spectrum processing for linearizing a PM MPL requires the step of phase modulation to intensity modulation (PM-IM) conversion to enable direct detection simultaneously with optical spectrum processing method for IMD3 suppression. Such a step can be achieved by adjusting the power ratio of OCB and second-order optical sideband (2 OSB), after filtering out optical carrier and one sideband [12] or tuning the phase of OCB and ±2 OSB [13]. However, these methods can only eliminate the IMD3 caused by third-order nonlinear distortion. To further reduce the IMD3 generated from higher order nonlinear distortion, an optical spectrum vector manipulation (OSVM) method should be implemented [14]. By taking multiple order OSBs into account and manipulating both the amplitude and phase of the OCB and OSBs, the IMD3 generated from third-order, fifth-order and even higher order nonlinear distortions can be eliminated simultaneously, which greatly increases the SFDR of the MPL.

Up to now, most of the linearization schemes based on optical spectrum processing are achieved by programmable optical processor based on liquid crystal on silicon (LCoS), which is bulky and costly. The potential of using integrated photonic circuits for manipulating the optical spectrum [15,16], has been shown to be advantageous for achieving advanced signal processing functionalities. It is thus important to investigate the feasibility of achieving link linearization with photonic circuits.

In this work, an optical spectrum processing scheme for PM MPL linearization based on Si_3N_4 integrated ring resonators is proposed. The phase and amplitude of the phase modulated signal are processed by four all-pass ring resonators for PM-IM conversion and IMD3 suppression. The experimental results show that an IMD3 suppression of 21.7 dB is achieved, and the SFDR is improved from 105.8 dB·Hz$^{2/3}$ to 112.7 dB·Hz$^{2/3}$, if the noise floor is maintained the same. Further, we analysis the limitation of using integrated ring resonators as processor and the noise performance of the proposed link. This work opens the way for on-chip linearization in MPLs.

2. Operation principle

The proposed phase modulated MPL is shown in Fig. 1. A programmable Si_3N_4 chip containing four all-pass ring resonator is used as an optical spectrum processor for linearization. The manipulation imposed to optical spectrum is determined by the tunable amplitude response $T(\omega)$ and phase response $\theta(\omega)$ of rings, which can be expressed as [17]

$$T(\omega)e^{j\theta(\omega)} = \frac{a - ce^{-j\phi(\omega)}}{1 - ace^{j\phi(\omega)}}e^{j[\pi+\phi(\omega)]}. \tag{1}$$

In Eq. (1), $c = \sqrt{1-k}$, $a = 10^{-\alpha L/20}$, k, α and $\emptyset$ are self-coupling coefficient, single-pass amplitude of the optical ring resonator, power coupling coefficient, propagation loss of optical waveguide (dB/cm), and round-trip phase respectively. There are three coupling state for all-pass ring resonator. When c = a, it operates at critical-coupling (CC) state. When c > a or c < a, it works at under-coupling (UC) or over-coupling (OC) state respectively. The phase shift of UC ring at resonant frequency is zero, while the phase shift of OC ring at resonant frequency is π, and can be changed continuously from 0 to 2π.

In this scheme, as shown in Fig. 1, the optical carrier is modulated by a two-tone radio frequency (RF) signal at PM. The modulated optical spectrum contains OCB and several OSBs. After amplification and adjusting the polarization state, the modulated optical signal is coupled into the programmable Si_3N_4 chip for optical spectrum processing. First, a single OC ring (ring 1) is used to impose 90 degrees phase shift at OCB for PM-IM conversion. After processing, the RF fundamental signal can be detected at photodetector with relatively large IMD3 components.

Optics EXPRESS

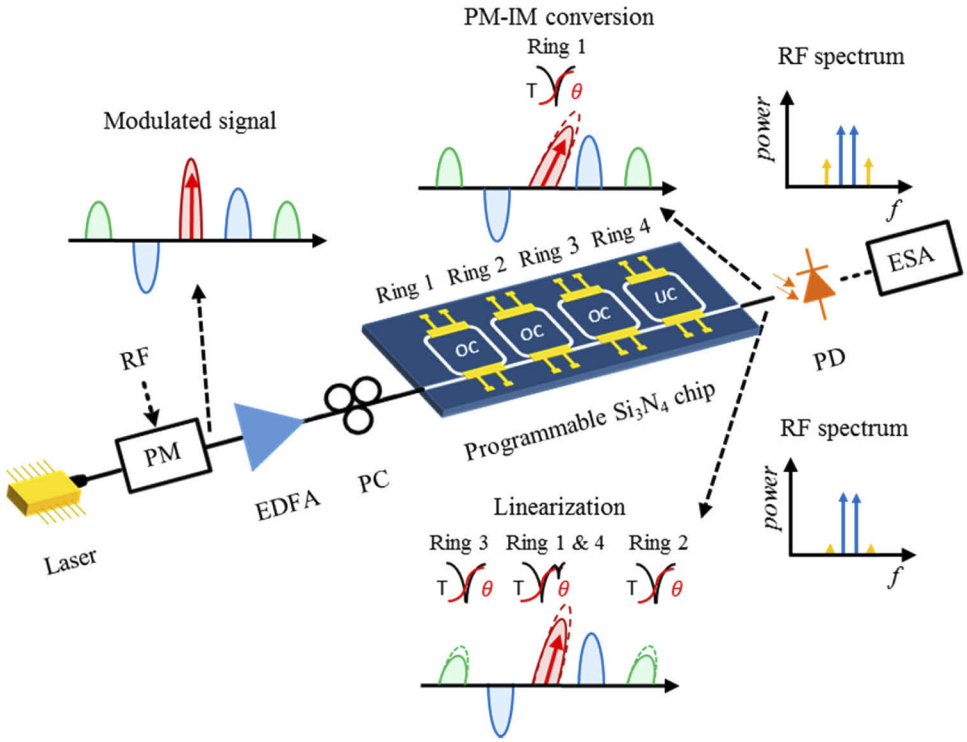

Fig. 1. Schematic of the proposed MPL. PM, phase modulator; PC, polarization control; OC, over-coupling; UC, under-coupling; EDFA, erbium-doped fiber amplifier; PD, photodetector; ESA, electronic spectrum analyzer.

This state of the link is measured as reference state without linearization. Then, an UC ring (ring 4) and two OC rings (ring 2 and ring 3) are added to OCB and ±2 OSB respectively. After carefully tuning the amplitude suppression and phase shift at OCB and ±2 OSB, the IMD3 terms generated from beating between different optical bands can add up destructively at photodetector.

We first investigate the primary optical spectral contributors of the IMD3 in a PM link by a two-tone analysis. The two-tone signal with amplitude of V_{RF} and angular frequencies of ω_1, ω_2 is expressed as $V_{in} = V_{RF}(\sin\omega_1 t + \sin\omega_2 t)$. Then it is modulated to the optical carrier by the PM. The output optical field of PM can be expressed as

$$E_{out}(t) = \sqrt{P_i}e^{j\omega_c t}e^{jm\sin\omega_1 t}e^{jm\sin\omega_2 t}, \tag{2}$$

where P_i, ω_c, $m = \pi V_{RF}/V_{\pi,RF}$, and $V_{\pi,RF}$ are the input optical power, angular frequency of the laser, the modulation index, and the RF half-wave voltage of PM. After applying Bessel function expansion of first kind to Eq. (2), we get

$$E_{out}(t) = \sqrt{P_i}e^{j\omega_c t}\sum_{n=-\infty}^{+\infty} J_n(m)e^{jn\omega_1 t}\sum_{k=-\infty}^{+\infty} J_k(m)e^{jk\omega_2 t}. \tag{3}$$

The power of higher order sidebands is quite small with small RF input signal, so here only zero to second order sidebands are taken into account for approximation.

The output optical spectrum of PM is illustrated in Fig. 2, including the OCB, the ±1 OSB and the ±2 OSB. The OCB contains the optical carrier and the even-order nonlinear components. The ±1 OSB is composed of the fundamental signal and odd-order distortion components,

Optics EXPRESS

while the ±2 OSB contains the even-order nonlinear components. There are three pairs of the main contributors for the IMD3. The first one is the beating of the optical carrier ω_c and $\omega_c + 2\omega_{1,2} - \omega_{2,1}$ ($\omega_c - 2\omega_{1,2} + \omega_{2,1}$). The second one is the beating between ±1 OSB of $\omega_c + \omega_{1,2}$ ($\omega_c - \omega_{1,2}$) and ±2 OSB of $\omega_c + 2\omega_{2,1}$ ($\omega_c - 2\omega_{2,1}$). The beating product between $\omega_c + \omega_{2,1} - \omega_{1,2}$ ($\omega_c - \omega_{2,1} + \omega_{1,2}$) and $\omega_c + \omega_{1,2}$ ($\omega_c - \omega_{1,2}$) is the third contributor. The sum of three beating products is the main part of the IMD3 in a PM link.

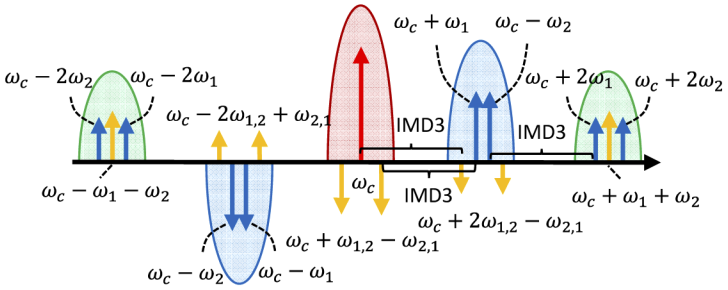

Fig. 2. Output optical spectrum of PM under two-tone test.

Optical field after processing by four ring resonators on programmable Si_3N_4 chip can be expressed as

$$E_p(t) = \sqrt{P_i}e^{j\omega_c t}\left\{\begin{array}{l} T_1(\omega_c)T_4(\omega_c)e^{j[\theta_1(\omega_c)+\theta_4(\omega_c)]}J_0J_0 \\ +T_1(\omega_c+\omega_{1,2}-\omega_{2,1})T_4(\omega_c+\omega_{1,2}-\omega_{2,1}) \\ \cdot e^{j[\theta_1(\omega_c+\omega_{1,2}-\omega_{2,1})+\theta_4(\omega_c+\omega_{1,2}-\omega_{2,1})]}J_{-1}J_1[e^{-j(\omega_1-\omega_2)t}+e^{j(\omega_1-\omega_2)t}] \\ +J_0J_1(e^{j\omega_1 t}+e^{j\omega_2 t}) \\ +J_{-1}J_2[e^{j(2\omega_1-\omega_2)t}+e^{j(2\omega_2-\omega_1)t}] \\ +J_{-1}J_0(e^{-j\omega_1 t}+e^{-j\omega_2 t}) \\ +J_{-2}J_1[e^{-j(2\omega_1-\omega_2)t}+e^{-j(2\omega_2-\omega_1)t}] \\ +T_2(\omega_c+2\omega_{1,2})e^{j\theta_2(\omega_c+2\omega_{1,2})}J_0J_2(e^{j2\omega_1 t}+e^{j2\omega_2 t}) \\ +T_2(\omega_c+\omega_1+\omega_2)e^{j\theta_2(\omega_c+\omega_1+\omega_2)}J_1J_1e^{j(\omega_1+\omega_2)t} \\ +T_3(\omega_c-2\omega_{1,2})e^{j\theta_3(\omega_c-2\omega_{1,2})}J_{-2}J_0(e^{-j2\omega_1 t}+e^{-j2\omega_2 t}) \\ +T_3(\omega_c-\omega_1-\omega_2)e^{j\theta_3(\omega_c-\omega_1-\omega_2)}J_{-1}J_{-1}e^{-j(\omega_1+\omega_2)t} \end{array}\right\}, \quad (4)$$

where $J_n = J_n(m)$ (n=0, ±1, ±2), $J_{-n} = (-1)^n J_n$. Amplitude response $T_i(\omega)$ and phase response $\theta_i(\omega)$ of the i-th ring resonator are given in Eq. (1). Here, we make an approximation that $T_i(\omega)$, $\theta_i(\omega)$ are constant in OCB or ±2 OSB for simplicity when the two-tone signals are close to each other, as shown in Fig. 3. The same amplitude suppression and phase shift are imposed to the ±2 OSB, which means $T_2 = T_3$ and $\theta_2 = \theta_3$.

When the processed optical signal expressed in Eq. (4) is sent to PD to retrieve the RF signal, the generated photo-current containing the fundamental and IMD3 components can be written as

$$I_{PD}(t) = R_{PD}|E_P(t)|^2 = I_1 \sin(\omega_{1,2}t) + I_3 \sin(2\omega_{1,2}t - \omega_{2,1}t), \quad (5)$$

where R_{PD} is responsivity of photodetector, $I_1$and I_3 denote the coefficients for fundamental signal and IMD3 components, which can be written as

$$I_1 = 4R_{PD}P_i[T_1T_4J_0^3J_1\sin(\theta_1+\theta_4) - T_2J_0^2J_1J_2\sin\theta_2 - T_1T_4J_0J_1^3\sin(\theta_1+\theta_4)], \quad (6)$$

Optics EXPRESS

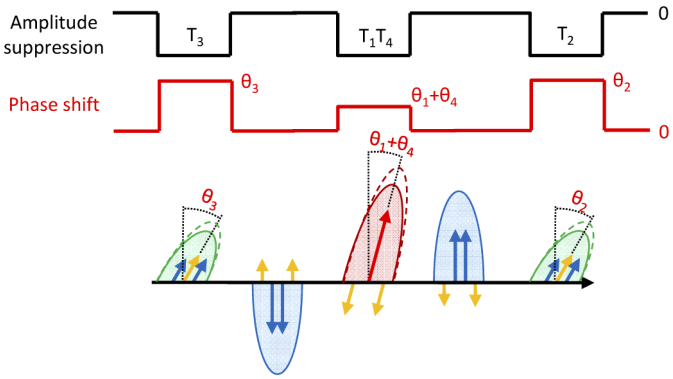

Fig. 3. Optical spectrum after processing.

$$I_3 = -4R_{PD}P_i[T_1T_4J_0^2J_1J_2\sin(\theta_1+\theta_4) + T_2J_0^2J_1J_2\sin\theta_2 + T_1T_4J_0J_1^3\sin(\theta_1+\theta_4)]. \quad (7)$$

The second and third terms in Eq. (6) are much smaller than the first term under small signal condition, so the I_1 can be approximately written as

$$I_1 = 4R_{PD}P_iT_1T_4J_0^3J_1\sin(\theta_1+\theta_4). \quad (8)$$

After applying Taylor series expansion to Eq. (7) and Eq. (8) to the third-order in m, I_1 and I_3 can be expressed as

$$I_1 = 2R_{PD}P_imT_1T_4\sin(\theta_1+\theta_4), \quad (9)$$

$$I_3 = -R_{PD}P_i\frac{m^3}{4}[3T_1T_4\sin(\theta_1+\theta_4) + T_2\sin\theta_2]. \quad (10)$$

It can be seen that the IMD3 distortion due to third-order nonlinearity will be minimized when the processing imposed to the OCB and ±2 OSB satisfy the condition:

$$3T_1T_4\sin(\theta_1+\theta_4) + T_2\sin\theta_2 = 0. \quad (11)$$

To minimize the IMD3 and maximize the fundamental signal simultaneously, a proper combination of T_1, θ_1, T_2, θ_2, T_4, θ_4 need to be found. We can choose $\sin(\theta_1+\theta_4) = -1/3$, $\sin\theta_2 = 1$, $T_1T_4 = T_2$, which means $\arcsin(-1/3) \approx 340.5°$ and 90° phase shifts are imposed to OCB and ±2 OSB respectively, and the amplitude suppression at OCB and ±2 OSB are equal. When the condition in Eq. (11) is met, I_1 will reduce to 1/3 of the original value, which will lead to a 9.54 dB power penalty of fundamental signal.

3. Simulation results

To verify our theoretical analysis, we simulate the performance of the proposed linearization methods. The parameters used in the simulation are as follows: input optical power of PM P_i = 18 dBm, RF input power P_{RF} = 3 dBm, insertion loss of PM L_{PM} = 4 dB, insertion loss of ring resonator chip L_{RR} = 8.5 dB, RF half-wave voltage $V_{\pi,RF}$ = 5 V, and responsivity of photodetector R_{PD} = 0.6 A/W. The response of ring resonator is expressed in Eq. (1). c and $\emptyset$ can be tuned to make the response of ring resonator get close to the condition in Eq. (11). Figures 4(a) and 4(b) are the responses of the rings used to process the OCB and ±2 OSB respectively. The marked points are the amplitude suppression and phase shift imposed to the OCB and ±2 OSB. The x axis of the figures are the frequency detuning from the center of OCB and ±2 OSB. The insets in Fig. 4 show that the phase shift and amplitude suppression are non-constant in the OCB and the ±2 OSB. There are phase differences of around 1.8 degrees

Optics EXPRESS

among the frequency components in OCB, and 2 degrees among the terms in ±2 OSB. The differences in amplitude suppression are around 0.05 dB in OCB and ±2 OSB. These non-constant responses can lead to a degradation in fundamental to IMD3 ratio, which will be discussed later.

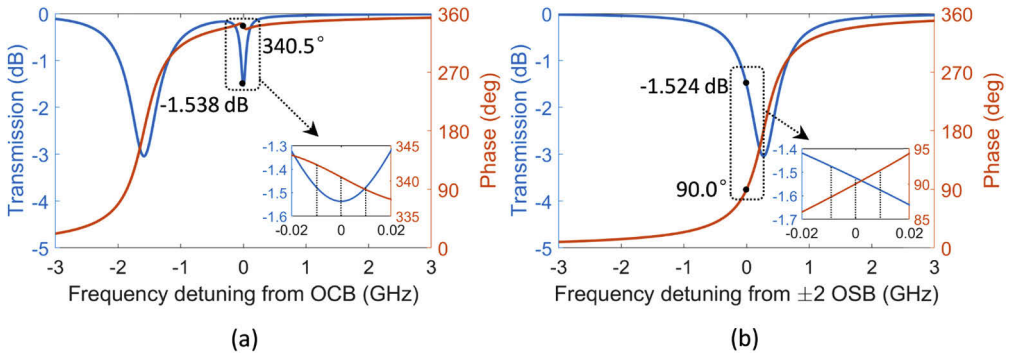

Fig. 4. (a) Response of the ring 1 and ring 4 used to process the OCB. (b) Response of the ring 2 or 3 used to process the ±2 OSB. The insets are the zoom-in figures at center of OCB and ±2 OSB.

In our simulation, a ring at OC state (ring 1) is used to impose a 90 degrees phase shift to the OCB for PM-IM conversion. After PM-IM conversion, the fundamental to IMD3 power ratio is about 30.4 dB as shown in Fig. 5(a). This state of the link is recorded as reference state without linearization. In the subsequent linearization process, an OC ring (ring 1) together with an UC ring (ring 4) are used to tailor OCB with a phase shift of 340.5 degrees and amplitude suppression around -1.5 dB, as shown in Fig. 4(a). In the meantime, two OC rings (ring 2, ring 3) are used to process ±2 OSB. The phase shift and amplitude suppression imposed to ±2 OSB are 90 degrees and around -1.5 dB, as illustrated in Fig. 4(b). After processing, the fundamental to IMD3 ratio is improved to 55.1 dB, which means IMD3 components are suppressed by 24.7 dB, as shown in Fig. 5(b). The simulation results indicate that the proposed method can effectively reduce the IMD3 components. An experiment is conducted in next section for further validation.

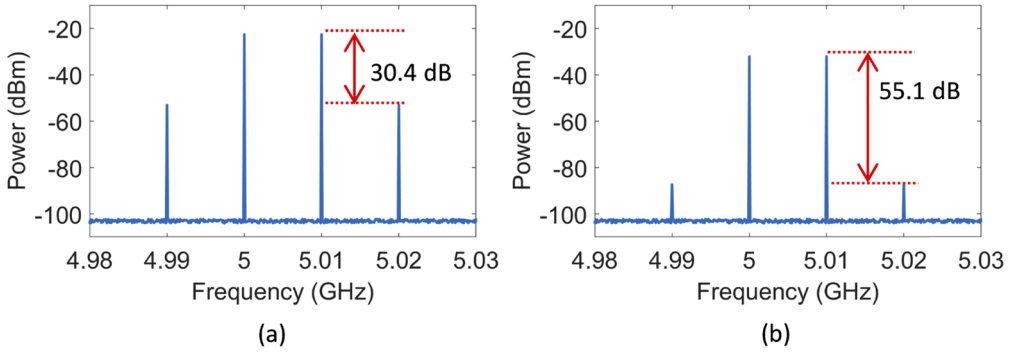

Fig. 5. Simulated RF spectrum (a) after IM to PM conversion (b) after linearization.

4. Experimental results

An experiment is performed to verify the proposed method, based on the schematic depicted in Fig. 1. An optical carrier from a laser (Pure Photonics PPCL550) operating at 1550 nm with an output power of 18 dBm is modulated by a phase modulator (Thorlabs 10 GHz) with optical

Optics EXPRESS

insertion loss of 4 dB. A two tone signal with frequency of 5 GHz and 5.01 GHz and power of 3 dBm is generated by signal generators (Wiltron 69147A and Rohde-Schwarz SMP02) and used to drive the phase modulator. The output of PM is amplified by a 2 W erbium-doped fiber amplifier (EDFA, Amonics), and then sent to a programmable silicon nitride chip (LioniX International) [18] for optical spectrum processing. The fiber-to-fiber insertion loss of the chip is 8.5 dB and the propagation loss of the waveguide is 0.15 dB/cm. The chip contains six all-pass ring resonators in series with a free spectral range (FSR) of 25 GHz (four of them are used). The coupling coefficient and resonance frequency of ring resonators can be tuned by using heaters to change the effective index of the waveguide. The processed optical signal is then sent to a photodetector (APIC 40 GHz Photodetector). The retrieved RF signal after photodetection is sent to a RF spectrum analyzer (Keysight N9000B) for measurement.

First of all, an OC ring is tuned to impose a phase shift of 90° at OCB for PM-IM conversion. The fundamental signal, IMD3 and SFDR of this PM-IM conversion link is measured as the reference without linearization. Then an OC ring and a UC ring are tuned to add a phase shift of $\theta_1 = \arcsin(-1/3) \approx 340.5°$at OCB. And phase shift of $\theta_2 = \arcsin(1) = 90°$ is imposed on the ±2 OSB by two OC rings respectively. The power of OCB and ±2OSB are attenuated by 1.5 dB to meet the condition in Eq. (11) for linearization. The optical power sent to PD remained constant at 5.5 dBm before and after linearization.

The measured electrical spectrum before and after linearization are shown in Fig. 6. The fundamental to IMD3 ratio without linearization is 32.6 dB as shown in Fig. 6(a). After the linearization, a fundamental to IMD3 ratio of 55.0 dB is achieved, which is 22.4 dB better than the link without linearization, as shown in Fig. 6(b). A power penalty of 10.2 dB at fundamental signal is observed in Fig. 6(b). The power penalty can be compensated by increasing the gain of the EDFA, as depicted in Fig. 6(c). After compensation, the optical power sent to PD is increased to 10.5 dBm, the fundamental to IMD3 ratio is 54.3 dB, which leads to an IMD3 suppression of 21.7 dB.

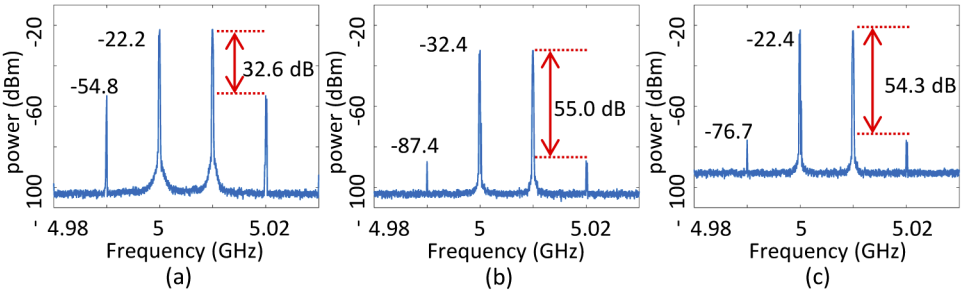

Fig. 6. Measured electrical spectrum after PD. (a) link without linearization (b) link with linearization (c) link with linearization and gain compensation.

SFDR before and after the linearization are measured as shown in Fig. 7. Output power of fundamental signal and IMD3 are plotted with the increase of input RF power. As depicted in Fig. 7, the SFDR of MPL before linearization is 105.8 dB·Hz$^{2/3}$ with a measured noise floor of -163.8 dBm/Hz, and the linearized MWP link is 106.9 dB·Hz$^{2/3}$ with a measured noise floor of -155.1 dBm/Hz. About 1 dB improvement is observed here, which mainly limited by the increase of the noise floor. The increase of noise floor is mainly caused by the increased optical power impinging to the photodetector. If we can compensate the power penalty of fundamental signal while maintaining the noise floor at the same level of link without linearization, the SFDR of the linearized link can reach 112.7 dB·Hz$^{2/3}$. We will further discuss the influence of noise floor in details in Section 5.2.

Optics EXPRESS

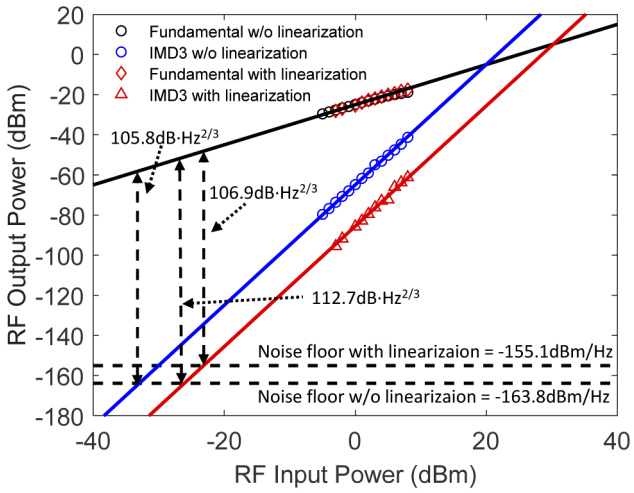

Fig. 7. Measured SFDR of the MPL without linearization and MPL with linearization.

5. Discussion

5.1. *Influence of non-constant amplitude and phase responses of ring resonator*

We achieved IMD3 suppression of 21.7 dB in the experiment, however, the slope of IMD3 power is still 3 after linearization instead of 5, as shown in Fig. 7, which means the IMD3 due to third-order nonlinearity is not eliminated completely. This is because the ring resonators cannot impose a constant amplitude suppression and phase shift in a certain bandwidth and the suppression and phase shift imposed by ring resonators are not independent as in the case of LCoS signal processor. These lead to limitations in perfectly satisfying the condition in Eq. (11), causing incomplete cancellation of the IMD3 component.

Here we discuss the influence of the non-flat/constant phase response and amplitude response in an optical band separately, as shown in Fig. 8. When we discuss the influence of phase response, the amplitude response is assumed to be flat and vice versa.

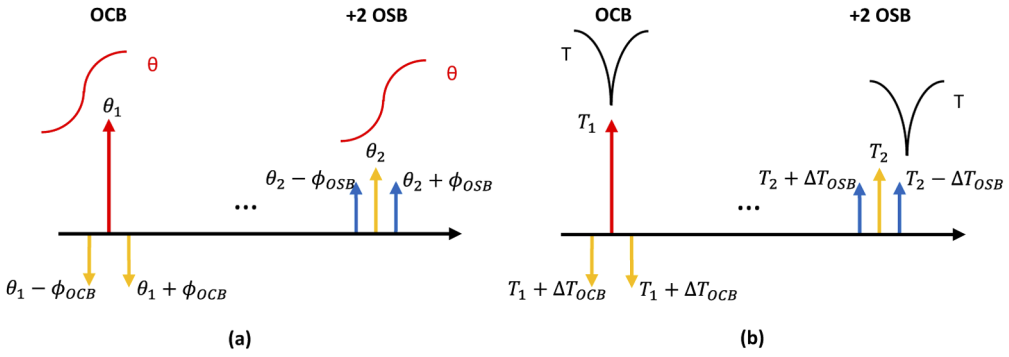

Fig. 8. Non-flat response of ring resonator (a) phase response (b) amplitude response.

We first simulate the influence of the non-flat phase response. As shown in Fig. 8(a), the phase shifts at the center of the OCB and 2 OSB are set as the desired value $\theta_1 = \arcsin(-1/3) \approx 340.5°$, $\theta_2 = \arcsin(1) = 90°$ respectively. The phase shifts of nonlinear distortion terms have a deviation

Optics EXPRESS

of ϕ_{OCB} and ϕ_{OSB} from the central frequency, which can be described as $\theta_1 - \phi_{OCB}$ and $\theta_2 - \phi_{OSB}$ at the lower frequency side and $\theta_1 + \phi_{OCB}$ and $\theta_2 + \phi_{OSB}$ at the higher frequency side.

The simulation results of fundamental to IMD3 ratio with the change of phase shift difference in OCB and ±2 OSB, namely ϕ_{OCB} and ϕ_{OSB}, are illustrated in Fig. 9. The highest fundamental to IMD3 ratio is achieved at $\phi_{OCB} = \phi_{OSB} = 0°$, which means the phase shifts in OCB and ±2 OSB are flat. Ideally at this point the IMD3 from third-order nonlinearity is completely canceled. The fundamental to IMD3 ratio decreases quickly when the phase differences in OCB and ±2 OSB increase, and the optimum point changed with the increase of the phase difference.

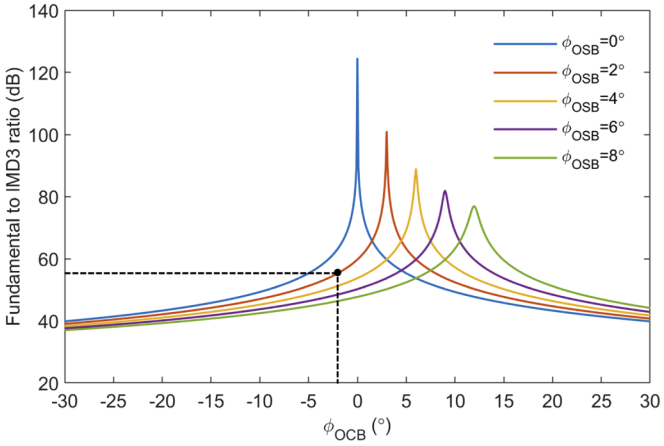

Fig. 9. Influence of non-flat phase response to the IMD3 suppression.

The non-flat amplitude suppression in OCB and ±2 OSB is also discussed. The amplitude suppression at center of the OCB and ±2 OSB is the desired value, in this case $T_1 = T_2 = -1.5\ dB$. As the resonance frequency of a UC ring is aligned to optical carrier at the center of OCB, the amplitude suppression of the nonlinear distortion terms at each side of the optical carrier is smaller than the suppression of optical carrier. The amplitude suppression of nonlinear distortion terms in OCB can be described as $T_1 + \Delta T_{OCB}$, as shown in Fig. 8(b). The suppression of nonlinear distortion terms at the lower frequency in ±2 OSB can be expressed as $T_2 + \Delta T_{OSB}$ and suppression of distortion terms at higher frequency in ±2 OSB can be expressed as $T_2 - \Delta T_{OSB}$. The fundamental to IMD3 ratio decreases quickly with the increase of amplitude suppression difference, namely ΔT_{OCB} and ΔT_{OSB}, as shown in Fig. 10.

Here, we compare the influence of the non-constant amplitude and phase responses of ring resonator with the simulation results in Section 3 to find the main factor that degrades the fundamental to IMD3 ratio. In our simulation at Section 3, phase differences among frequency components in OCB and ±2 OSB are around $\phi_{OCB} = -1.8°$, $\phi_{OSB} = 2°$ respectively, and the amplitude suppression differences are around 0.05 dB, leading to a fundamental to IMD3 ratio around 55 dB, as shown in Fig. 5. If there are only phase differences of $\phi_{OCB} = -1.8°$ and $\phi_{OSB} = 2°$, the fundamental to IMD3 ratio is around 56 dB, as depicted in Fig. 9. If only amplitude suppression differences exist, suppression differences around 0.05 dB at OCB and ±2 OSB result in a 79 dB fundamental to IMD3 ratio, as illustrated in Fig. 10. The fundamental to IMD3 ratio in the simulation at Section 3 is close to the result in Fig. 9, where only phase shift differences are considered, which means the degradation of fundamental to IMD3 ratio is mainly dominated by the phase shift differences in each optical band in our method.

Optics EXPRESS

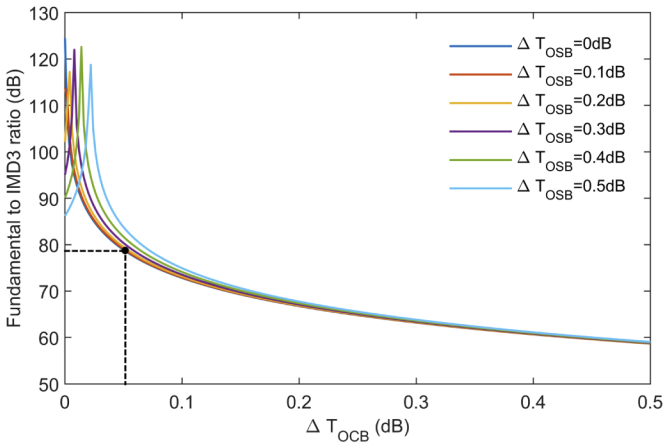

Fig. 10. Influence of non-flat amplitude response to the IMD3 suppression.

5.2. *Influence of noise*

The SFDR will be influenced by IMD3 suppression and the noise floor of the link, namely noise power spectral density (PSD) of the link. In our proposed linearization method, the SFDR performance is not only limited by the non-flat response of ring resonator but also the increase of noise PSD of the link. The noise PSD of the link consists of several noise sources, for example the thermal noise, the shot noise, relative intensity noise (RIN), amplified spontaneous emission from the EDFA and the phase noise from the laser that is converted to intensity noise by the ring resonator. The PSD of the thermal noise sent to a matched load in W/Hz can be expressed as

$$S_{th} = (1 + g_{MPL})k_B T, \tag{12}$$

where g_{MPL} is the MPL gain, k_B is the Boltzmann constant and T is the environment temperature in Kelvin. The shot noise PSD can be written as

$$S_{shot} = 2qI_d R_L \tag{13}$$

where q is the electron charge, I_d is average detected photocurrent and R_L is the load resistance. The noise from EDFA and the phase noise converted to intensity noise can be regarded as the additional RIN to the system [19,20]. Here we define the total RIN (RIN_{tot}) as the sum of the RIN from the laser (RIN_{laser}), the ASE noise (RIN_{ASE}) and the phase noise (RIN_{phase}) as [21] did,

$$RIN_{tot} = RIN_{laser} + RIN_{ASE} + RIN_{phase} \tag{14}$$

The noise PSD of the system RIN can thus be expressed as

$$S_{RIN_{tot}} = RIN_{tot} I_d^2 R_L. \tag{15}$$

In a MPL where the output of PD is impedance matched, the total noise PSD is

$$S_{noise} = S_{th} + \frac{1}{4}(S_{shot} + S_{RIN_{tot}}). \tag{16}$$

The measured noise PSD at the different link state are listed in Table 1.

Using Eqs. (12), (13), (15) and (16) and the measured data of optical power at PD and the noise PSD listed in Table 1, the RIN_{tot} for each state can be extracted, which are also listed in Table 1.

Optics EXPRESS

Table 1. Measured noise performance.

Link state	Optical power at PD (dBm)	Calculated photocurrent (mA)	Noise PSD (dBm/Hz)	RIN_{tot} (dB/Hz)
PM-IM link	5.5	3.3	-163.8	-152.9
Linearized link	10.5	6.3	-155.1	-153.1
PM link	5.5	3.3	-168.1	-163.1
PM link	10.5	6.3	-160.1	-159.3

First, the impact of phase noise to intensity noise conversion is analyzed. The PM link with 5.5 dBm optical power at photodetector has the lowest noise PSD and RIN_{tot}, as there is no phase noise converted to intensity noise from laser in PM links. In PM-IM link, a ring resonator is used to process optical carrier for PM-IM conversion. The ring resonator will convert phase noise of laser to intensity noise, which increases the noise PSD and RIN_{tot} to -163.8 dBm/Hz and -152.9 dB/Hz respectively.

In linearized link, to compensate the power penalty at fundamental signal, optical power send to the photodetector need to be increased from 5.5 dBm to 10.5 dBm. This further increase the noise PSD to -155.1 dBm/Hz.

Then the main contributor of RIN in the system is analyzed. Substituting the total RIN of linearized link $RIN_{tot_{linearized}}$ and PM link $RIN_{tot_{PM}}$ into Eq. (14), we can calculate the $RIN_{phase} = -154.2$ dB/Hz. The RIN comes from the laser and ASE of EDFA can be extract as $RIN_{laser+EDFA} = -159.3$ dB/Hz, according to Eq. (14). In this case, the main contributor of RIN in our proposed linearized link is phase noise to intensity noise conversion of the laser. The RIN_{phase} is proportional to the linewidth ($\Delta\nu$) of the laser [20], which is in the order of 10 KHz for the laser used in the experiments. Thus, to reduce the RIN_{phase} contribution to the system noise, a laser with narrower linewidth can be used. As an example, using a laser with a linewidth of 1 kHz, which is already commercially available, the RIN_{phase} can be reduced from -154.2 dB/Hz to -164.2 dB/Hz.

The RIN comes from the laser and ASE of EDFA can be reduced by using a low RIN, high power laser without EDFA. Currently the laser with RIN as low as -170 dB/Hz is available. In this case, if a narrow linewidth (1 KHz), low RIN (-170 dB/Hz), high power laser is used in the link. The RIN of the link is dominated by the RIN_{phase} (-164.2 dB/Hz). The calculated noise PSD in PM-IM conversion link is -168.3 dBm/Hz (5.5 dBm optical power into PD) and the linearized link is -162.8 dBm/Hz (10.5 dBm optical power into PD), which lead to an SFDR improvement from 108.9 dB·$Hz^{2/3}$ to 112.0 dB·$Hz^{2/3}$. In this case, these two links have the same link gain of -25.2 dB.

To further limit the increase of noise PSD for SFDR improvement, the optical carrier suppression technique can be implemented. By suppressing the optical carrier and amplifying the optical sideband, this method can improve the link gain while maintaining the optical power sent to the photodetector the same, which will also maintain the noise floor of the link [22].

6. Conclusion

A novel on-chip optical spectrum processing method to improve the linearity of the phase modulated MPL is proposed and demonstrated. By properly manipulating the phase and amplitude of OCB and ±2 OSB, the IMD3 can be suppressed. Experimental results show an IMD3 suppression of 21.7 dB. SFDR is improved from 105.8 dB·$Hz^{2/3}$ to 112.7 dB·$Hz^{2/3}$, if the noise floor is maintained the same. This method uses Si_3N_4 integrated ring resonators instead of LCoS based processor for optical spectrum processing, which will reduce the footprint and complexity of a linearized MPL. Furthermore, the optical spectrum processing method can also be used for advanced signal processing functions with the same building blocks [23]. So it is possible to combine linearization and advanced functionalities in the same integrated platform,

Optics EXPRESS

which will greatly reduce the complexity and cost of a linearized microwave photonic system. The proposed on-chip linearization method is highly promising in radio-over-fiber system for transmitting high speed, large bandwidth RF signal.

Funding

Nederlandse Organisatie voor Wetenschappelijk Onderzoek (Start Up (740.018.021)); Stichting voor de Technische Wetenschappen (Vidi 15702); China Scholarship Council.

Disclosures

The authors declare no conflict of interest.

References

1. J. Capmany and D. Novak, "Microwave photonics combines two worlds," Nat. Photonics **1**(6), 319–330 (2007).
2. J. Yao, "Microwave Photonics," J. Lightwave Technol. **27**(3), 314–335 (2009).
3. V. J. Urick Jr, J. D. Mckinney, and K. J. Williams, *Fundamentals of Microwave Photonics* (John Wiley & Sons, 2015), Chap. 2.
4. E. I. Ackerman, "Broad-band linearization of a Mach-Zehnder electrooptic modulator," IEEE Trans. Microw. Theory Tech. **47**(12), 2271–2279 (1999).
5. B. M. Haas, V. J. Urick, J. D. McKinney, and T. E. Murphy, "Dual-Wavelength Linearization of Optically Phase-Modulated Analog Microwave Signals," J. Lightwave Technol. **26**(15), 2748–2753 (2008).
6. W. Zhang, A. Wen, X. Xu, W. Zhai, K. Wei, and H. Zhang, "Dual-wavelength linearization of analog photonic link based on PM–IM conversion," Opt. Commun. **420**, 174–178 (2018).
7. M. Huang, J. Fu, and S. Pan, "Linearized analog photonic links based on a dual-parallel polarization modulator," Opt. Lett. **37**(11), 1823–1825 (2012).
8. Q. Tan, Y. Gao, Y. Fan, and Y. He, "Multi-octave analog photonic link with improved second- and third-order SFDRs," Opt. Commun. **410**, 685–689 (2018).
9. J. Dai, K. Xu, R. Duan, Y. Cui, J. Wu, and J. Lin, "Optical linearization for intensity-modulated analog links employing equivalent incoherent combination technique," in *2011 International Topical Meeting on Microwave Photonics Jointly Held with the 2011 Asia-Pacific Microwave Photonics Conference* (IEEE, 2011), pp. 230–233.
10. Y. Cui, Y. Dai, F. Yin, J. Dai, K. Xu, J. Li, and J. Lin, "Intermodulation distortion suppression for intensity-modulated analog fiber-optic link incorporating optical carrier band processing," Opt. Express **21**(20), 23433–23440 (2013).
11. W. Zhu, J. Hu, Y. Gu, F. Fan, Z. Kang, X. Han, and M. Zhao, "Dynamic Range Improvement of a Microwave Photonic Link Based on Brillouin Processing," IEEE Photonics Technol. Lett. **28**(23), 2681–2684 (2016).
12. P. Li, L. Yan, T. Zhou, W. Li, Z. Chen, W. Pan, and B. Luo, "Improvement of linearity in phase-modulated analog photonic link," Opt. Lett. **38**(14), 2391–2393 (2013).
13. J. Li, Y. Zhang, S. Yu, and W. Gu, "Optical Sideband Processing Approach for Highly Linear Phase-Modulation/Direct-Detection Microwave Photonics Link," IEEE Photonics J. **6**(5), 1–10 (2014).
14. R. Wu, T. Jiang, S. Yu, J. Shang, and W. Gu, "Multi-Order Nonlinear Distortions Analysis and Suppression in Phase Modulation Microwave Photonics Link," J. Lightwave Technol. **37**(24), 5973–5981 (2019).
15. K. Takiguchi, K. Okamoto, T. Kominato, H. Takahashi, and T. Shibata, "Flexible pulse waveform generation using silica-waveguide-based spectrum synthesis circuit," Electron. Lett. **40**(9), 537–538 (2004).
16. X. Guo, T. Yin, Y. Liu, B. Morrison, C. Cantaloube, W. Bogaerts, B. J. Eggleton, D. Marpaung, and A. C. Bedoya, "All-Integrated Universal RF Photonic Spectral Shaper," in *Asia Communications and Photonics Conference* (Optical Society of America, 2019), paper M4D.7.
17. W. Bogaerts, P. De Heyn, T. Van Vaerenbergh, K. De Vos, S. Kumar Selvaraja, T. Claes, P. Dumon, P. Bienstman, D. Van Thourhout, and R. Baets, "Silicon microring resonators," Laser Photonics Rev. **6**(1), 47–73 (2012).
18. C. G. H. Roeloffzen, M. Hoekman, E. J. Klein, L. S. Wevers, R. B. Timens, D. Marchenko, D. Geskus, R. Dekker, A. Alippi, R. Grootjans, A. van Rees, R. M. Oldenbeuving, J. P. Epping, R. G. Heideman, K. Wörhoff, A. Leinse, D. Geuzebroek, E. Schreuder, P. W. L. van Dijk, I. Visscher, C. Taddei, Y. Fan, C. Taballione, Y. Liu, D. Marpaung, L. Zhuang, M. Benelajla, and K. J. Boller, "Low-Loss Si3N4 TriPleX Optical Waveguides: Technology and Applications Overview," IEEE J. Sel. Top. Quantum Electron. **24**(4), 1–21 (2018).
19. V. J. Urick, M. E. Godinez, P. S. Devgan, J. D. McKinney, and F. Bucholtz, "Analysis of an Analog Fiber-Optic Link Employing a Low-Biased Mach–Zehnder Modulator Followed by an Erbium-Doped Fiber Amplifier," J. Lightwave Technol. **27**(12), 2013–2019 (2009).
20. J. M. Wyrwas and M. C. Wu, "Dynamic Range of Frequency Modulated Direct-Detection Analog Fiber Optic Links," J. Lightwave Technol. **27**(24), 5552–5562 (2009).
21. D. Marpaung, C. Roeloffzen, A. Leinse, and M. Hoekman, "A photonic chip based frequency discriminator for a high performance microwave photonic link," Opt. Express **18**(26), 27359–27370 (2010).

Optics EXPRESS

22. O. Daulay, R. Botter, and D. Marpaung, "On-chip programmable microwave photonic filter with an integrated optical carrier processor," OSA Continuum **3**(8), 2166–2174 (2020).
23. O. Daulay, G. Liu, X. Guo, M. Eijkel, and D. Marpaung, "A Tutorial on Integrated Microwave Photonic Spectral Shaping," J. Lightwave Technol. (2020), In press.